

Shear strengthening of deficient RC deep beams using NSM FRP system: Experimental and numerical investigation

Aref Abadel*

Department of Civil Engineering, College of Engineering, King Saud University,
Riyadh 11421, Saudi Arabia

It is essential to retrofit deep beams with shear inadequacies because these beams, although they have the same shear and flexural reinforcements as ordinary beams, are more susceptible to shear failure. Hence, it is of great significance to overcome the shear weaknesses in deep beams. This research paper aims to experimentally examine the effectiveness of near-surface mounted (NSM) carbon fiber reinforced polymer (CFRP) for retrofitting reinforced concrete (RC) deep beams subjected to shear forces. The study involved three different types of specimens. The first specimen was constructed with concrete throughout its span and included shear stirrups. The second specimen was divided into two halves, with one half lacking shear reinforcements and the other half having them. The third specimen had steel web reinforcement in one half of the span, while the other half was strengthened using NSM CFRP U-wrap strips and externally bonded horizontal CFRP strips. The proposed strengthening method significantly increased the shear strength of the deep beams, surpassing that provided by steel web reinforcement alone. Furthermore, the NSM CFRP strengthened specimen exhibited a change in failure mode from shear to flexural failure. In comparison to the control beam without stirrups, the beams strengthened with NSM CFRP U-wrap strips demonstrated an impressive 82% improvement in shear strength, while the beam with shear reinforcement showed a 23 % enhancement in load capacity. The proposed strengthened scheme is capable of enhancing the structural performance and load-carrying capacity effectively. A finite element model was generated utilizing ABAQUS software to simulate the behavior of the tested deep beams and verified against the experimental outcomes. The numerical models successfully predicted the behavior of the RC deep beams strengthened with NSM CFRP when compared to the experimental data.

Keywords: *deep beam, shear, strengthening, carbon fiber reinforced polymer, near surface mounted, numerical*

1. Introduction

Deep beams are commonly utilized in reinforced concrete structures such as garages, bridges, reservoirs, etc. Deep beams, subjected to significant shear stresses due to their specific shape and loading conditions, necessitate considerable attention to resolve any deficiencies in their structural strength. The shear deficiencies in deep beams, caused by poor reinforcement details, corrosion, insufficient concrete strength, and variations in loading circumstances over time, necessitate the strengthening of these beams. To address the reduced shear capacity caused by the lack of shear reinforcements and other factors, different methods are employed to strengthen the beams.

Fiber-reinforced polymers (FRPs) are commonly employed to enhance the strength of different structures owing to their favorable characteristics [1–5]. The typically utilized FRPs for strengthening purposes refer to carbon-fiber-reinforced polymer (CFRP), glass-fiber-reinforced polymer (GFRP), basalt-fiber-reinforced polymer (BFRP), and composites of natural fiber-reinforced polymer. Research studies consistently show that the NSM technique has superior efficiency in strengthening compared to the externally bounded reinforcement (EBR) technique when using CFRP sheets [6]. Beyond the utilization of FRPs as a strengthening material, researchers may also investigate the incorporation of fibers into composites or construction materials other than cement mortars, including concrete, in order to tackle particular challenges or satisfy changing industry demands

* E-mail: aabadel@ksu.edu.sa

[7, 8]. However, Multiple shear-strengthening strategies, including FRP, and their effects on the response of RC deep beams have been investigated [9–11]. Akkaya et al. [12] examined the shear performance of reinforced concrete deep beams with short spans that were strengthened using fiber-reinforced polymer (FRP) strips. The study demonstrates that the utilization of FRP strips enhances the shear capacity and behavior of reinforced concrete deep beams. Islam et al. [13] analyzed the shear behavior of RC deep beams by using externally bonded FRP sheets, which are commonly used for shear strengthening of inadequate RC beams (e.g. [14–16]). The results of their tests showed that the various strengthening strategies increased the failure stress of the beam and slowed the spread of diagonal cracks. However, a particular experiment in this area demonstrated a significant enhancement in the resistance to shearing forces of rectangular deep beams when externally bonded CFRP systems were utilized. Li and Leung [16] investigated the shear behavior of deep beams that were strengthened using full wrapping strips of FRP across various shear spans. The researchers concluded that the increase in shear capacity of concrete deep beams is significantly affected by the ratio of the shear span to effective depth. Adhikary and Mutsuyoshi [17] conducted an experiment in which they put eight concrete deep beams strengthened with unidirectional carbon FRP (CFRP) laminates to the test. The shear strength of the vertical U-wrapped beams was found to be nearly double that of the unreinforced beam counterpart. Albidah et al. [18] focused on strengthening shear-deficient RC deep beams. Through experiments and analysis, they found that techniques such as external steel plates, FRP wraps, and NSM FRP effectively improved the shear capacity of the beams, enhancing their structural performance and load-carrying capacity. Godat and Chaallal [19] introduced an analysis and design approach for girders that are strengthened in shear using CFRP, which utilizes the strut-and-tie model. The method proposed by the authors integrates the consideration of tensile forces in both steel shear reinforcements and externally bonded CFRP laminates. Tanaka [20] tested the shear

strength of CFRP-reinforced deep beams. They discovered that the effective bond length of the CFRP bars affected the failure mode as well as the bond between the CFRP bars and the concrete substrate. The previous study demonstrated the significance of the shear-strengthening method. Hanoon et al. [21] investigated RC deep beams reinforced in shear with FRP. Externally bonded CFRP sheets were used to reinforce the beams under shear. The test findings were used to create a simpler strut-and-tie model for calculating shear strength. Abadel et al. [10, 22, 23] investigated how carbon fiber-reinforced polymer (CFRP) improved the shear response of ultra-high-performance fiber-reinforced concrete (UHPFRC) deep beams. The CFRP reinforcement improved the beams' overall structural performance by increasing load-carrying capacity, crack resistance, stiffness, and ductility. However, many further studies [24–26] examined the shear response of deep beams with different configurations and materials. Jedrzejko et al. [27] performed a detailed investigation of strength models used for strengthening RC beams with near-surface mounted (NSM) fiber-reinforced polymer (FRP). Their study significantly enhances our understanding of the performance of NSM FRP strengthened beams. In summary, the NSM FRP technique has benefits such as easy installation, increased bond durability, and better protection of FRP reinforcements by the concrete cover. This makes it a good approach for reinforcing deep beams and other structural elements [25]. The approach has undergone extensive research and implementation worldwide, demonstrating its efficacy in improving the performance and longevity of reinforced concrete structures. The aforementioned review reveals a lack of extensive research on the behavior of reinforced concrete (RC) deep beams retrofitted using various methods. While there have been studies investigating the shear response of concrete deep beams, further research is needed regarding the strengthening of RC deep beams using the near-surface mounted (NSM) technique. Therefore, the purpose of this study was to examine the efficiency of NSM retrofitting schemes using CFRP strips in improving the shear resistance of concrete and RC deep beams.

2. Experimental Program

2.1. Mixture Proportions and Material Properties

According to Table 1, beams were developed with a targeted compressive strength of 65 Mpa. Standard concrete cylinders, on the other hand, averaged a compressive strength of 68.5 Mpa after 28 days. Tables 2 and 3 list the typical characteristics of steel rebars and strengthening materials properties such as carbon fiber-reinforced polymer (CFRP) sheets, epoxy primer, and Sikadur 31 thixotropic epoxy resin mortar, respectively.

2.2. Test specimens

The experimental program described in this paper comprised results from three RC deep beam bending tests. The beams were supported on rigid steel rollers of 75 mm diameter and subjected to a static point load applied at the mid-span of the beam. Beams were rectangular in cross-section (100 mm width and 250 mm depth) with overall and effective span lengths of 1000 mm and 850 mm, respectively. All beams had a typical

Table 1. Mixture composition of concrete mixture

Material	Weight (kg/m ³)
Cement	650
Silica sand	528
Coarse aggregate (Nominal size = 10 mm)	770
Crush sand	264
Water (w/c = 0.25)	162.5
Super-plasticizer(Gli-110)	3 Liters

Table 2. Mechanical characterization of steel reinforcement

Mechanical Property	Bar diameter		Test Standard
	10 mm	6 mm	
Yield strength, (MPa)	525	280	ASTM A370 (2017)
Ultimate strength, (MPa)	578	380	
Modulus of elasticity, (GPa)	200	200	

Table 3. Characteristics of the strengthening materials

Item	Value
CFRP composite	
Type of FRP	Unidirectional CFRP sheet
Longitudinal elastic modulus of the primary fibers. (GPa)	77.3
Transverse elastic modulus relative to the primary fiber direction. (MPa)	40.6
Strain at fracture along the primary fiber direction (%)	1.1
Maximum tensile strength along the primary fiber direction (MPa)	846
Thickness of each individual layer, t_f (mm)	1.0
Epoxy	
Density (kg /l)	1.16
Tensile strength of the adhesive (MPa)	> 4.0 (7 days)
Tensile modulus of elasticity (GPa)	3.5 (7 days)
Sikadur_31 Thixotropic epoxy_resin mortar	
Tensile strength of the adhesive (MPa)	15
Density (kg /l)	1.65
Modulus of Elasticity (GPa)	4.3

longitudinal reinforcement placed in two layers with 20 mm clear spacing, each comprising 2 ϕ 10 deformed steel bars. Horizontal web steel of 2 ϕ 6 was provided at the mid-height of the beam. One layer of compression steel 2 ϕ 6 was also placed mainly to hold the shear stirrups. Bottom steel was arranged in a U-shape to avoid anchorage issues as detailed in Figure 1. Clear concrete cover of 25 mm was adopted for all sides of the beam cross-section.

Shear reinforcement of the beams was considered the main variable of the test program. The first beam (DB-S-F) incorporated two-legged f6 mm plain steel shear stirrups distributed equally along the full span of the beam with center to center spacing of 100 mm. The second beam (DB-NS) is the same as SF0-F, but stirrups were distributed only in

Table 4. Overview of test samples

Specimen	Left half span			Right half span
	Shear stirrups	Shear strengthening	Shear stirrups	Shear strengthening
DB-S-F	2L-f6@100	None	2L-f6@100	None
DB-NS0	2L-f6@100	None	None	None
DB-FRP	2L-f6@100	Yes	None	The specimen has two layers of U-wraps of FRP (25 mm wide) spaced at 100 mm intervals, along with a single layer of horizontally bonded FRP strips (50 mm wide) placed at the mid-depth on each face.

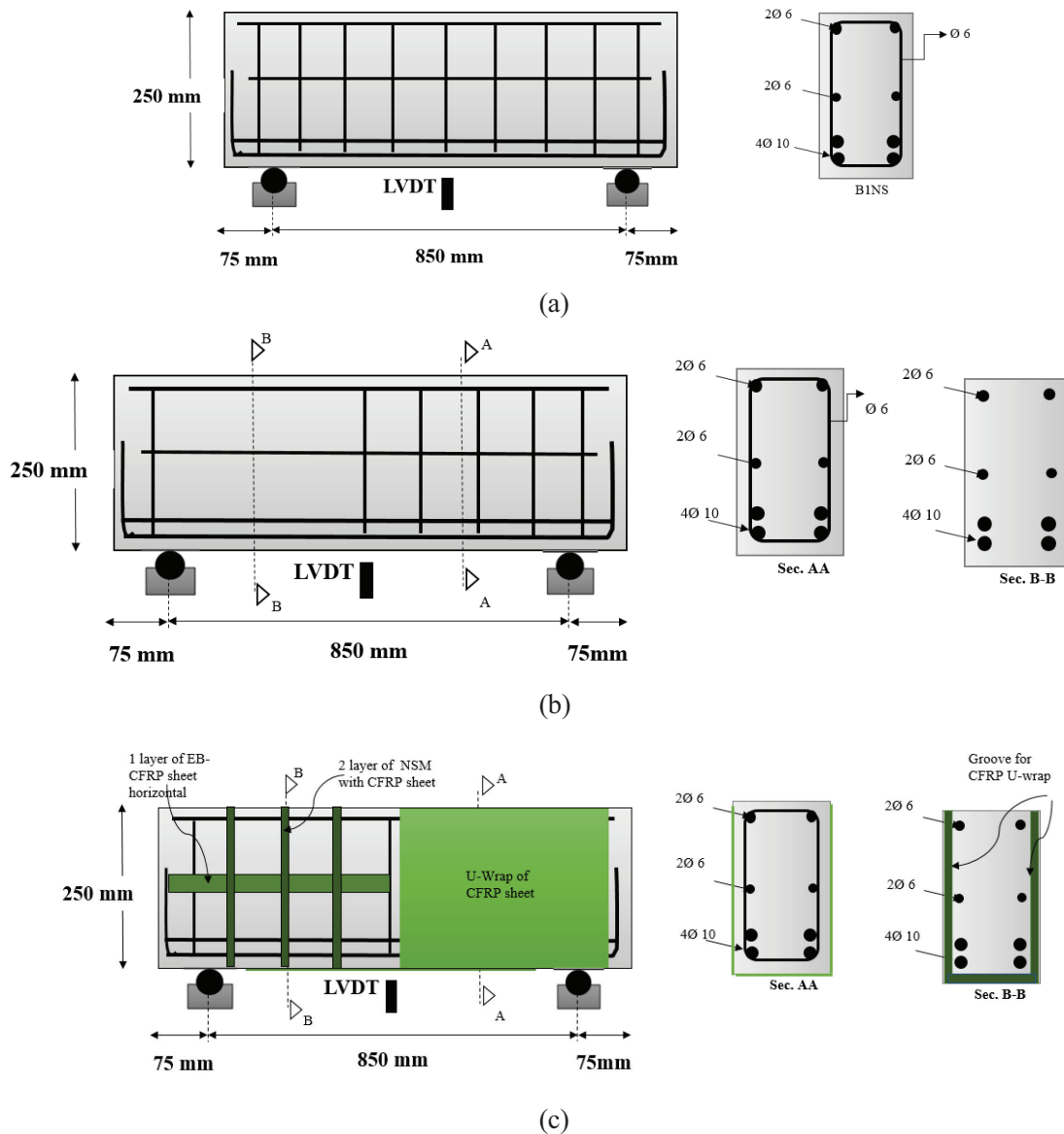


Fig. 1. Test specimens: (a) DB-S-F; (b) DB-NS0; and (c) DB-FRP. (All dimensions are in mm)

one half of the span, while the other half had no stirrups. It should be noted that beam SF0 was tested as a control as a part of a previous experimental program as detailed in Albidah et al. [18] and will be reported throughout this paper for the purpose of comparison with the other two specimens.

The third beam (DB-FRP) was the same as DB-NS but with FRP strengthening. For the half span of the beam with no shear reinforcements, near surface-mounted U-wraps of unidirectional CFRP strips. Two layers of the strips were provided in 25 mm wide grooves with a depth of 25 mm at a spacing of 100 mm. Following the epoxy setting of the CFRP U-wraps with the concrete, thixotropic epoxy resin mortar was used to fill and level the grooves. The centerline of the CFRP U-wraps fits the position of the missing shear reinforcements from the half span of the beam. A horizontal CFRP strip of 50 mm width was externally bonded at mid-height of the beam. The horizontal strip extended from the beam end to the mid-span at both faces. In order to properly quantify the shear resistance of the repaired section of the beam, it was necessary to upgrade both the shear capacity of the other half of the span (which is half steel stirrups) and the beam flexural capacity. Therefore, the half span of the beam having shear reinforcements was retrofitted using one layer of externally bonded full U-wrap. Also, two layers of CFRP strips were externally bonded to the soffit of the beam along the whole span length of the beam. Details of the beams are presented in Figure 1.

2.3. Instrumentations and test procedure

The beams underwent testing using a three-point bending setup. A concentrated load was applied at the center of the beam, and this load was gradually increased until the beam failed. The loading process was controlled by displacements and maintained a rate of 0.5 mm/min. To measure the displacement of the beam, a linear variable displacement transformer (LVDT) was installed beneath the midpoint of the beam. Strain gauges were placed on steel stirrups, two layers of bottom steel, and CFRP (carbon fiber reinforced polymer) sheet and strips, as shown in Figure 2. All beams

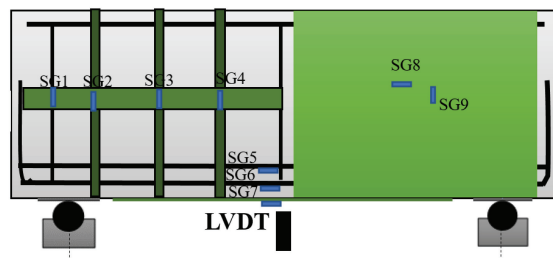


Fig. 2. Strain gauge locations

had strain gauges (SG-1, SG-2, SG-3, SG 4, SG-5, and SG-6) attached to common locations on the steel rebars, as depicted in Figure 2. However, in the case of the BD-FRP specimen, additional strain gauges were attached to the CFRP flexural sheet (SG-7) and the horizontal and vertical strips (SG-8 and SG-9).

3. Test results and findings

3.1. Failure modes of deep beams

3.1.1. DB-S-F specimen

This specimen of deep beam (DB-S-F) is typically designed to be sufficient with shear and flexural reinforcement. These deep beams demonstrate a predominance of shear behavior, indicating that shear forces have a more significant influence on their structural response compared to flexural forces than what was observed in these reference specimens. However, at approximately the midpoint between the support and loading point, two inclined cracks were initiated on both sides of the beam when the load reached around 65 kN. With further load increment, the right-hand side (RHS) crack propagated upward. As the load continued to increase, new shear cracks formed and spread. Notably, a prominent shear crack emerged along the left-hand side strut, extending from the loading point to the support, when the load reached approximately 116 kN. This crack played a dominant role in determining the behavior and failure mode of the beam, although minor shear and flexural cracks appeared as the load approached its peak. Therefore, the failure mode of this beam can be described as a mixed shear mode of failure, distinguished

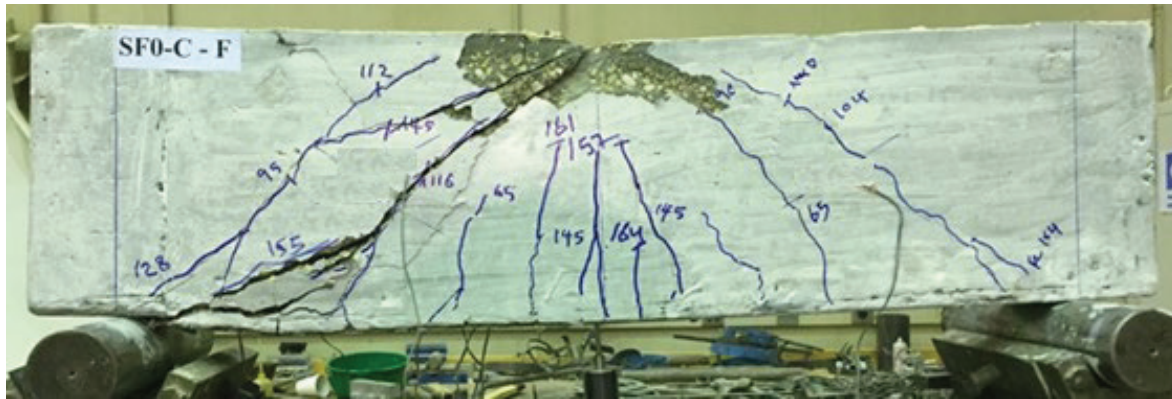


Fig. 3. Failure pattern of specimen DB-S-F



Fig. 4. Failure pattern of specimen DB-NS0

by diagonal splitting and shear compression, as depicted in Figure 3.

3.1.2. DB-NS specimen

The initial flexural crack was identified in the unreinforced shear section when the load reached 48 kN. Subsequently, another flexural crack appeared on the opposite side of the beam as the load increased to 57 kN. Upon reaching 80 kN, a diagonal shear crack started in the section of the beam that lacked sufficient shear strength, gradually widening until the beam ultimately failed. Figure 4 illustrates that the predominant failure mode of the beam is noted as a diagonal shear failure.

3.1.3. DB-FRP specimen

The flexural cracks were initially observed at a load level of 105 kN in the middle of the beam span. At a load of 167 kN, minor cracks start appearing in the NSM strengthened portion. Due to the coverage of CFRP sheets and strips on a significant portion of half of the beam, it was not possible to monitor the crack development. During failure, only a few minor shear cracks were observed in the NSM-U-wrap strips section of the deep beam (Fig. 5). There was no debonding observed in the vertical section covered by the full-wrap CFRP sheet. Overall, the beam primarily failed in flexure-shear mode. However, at the ultimate load, a major

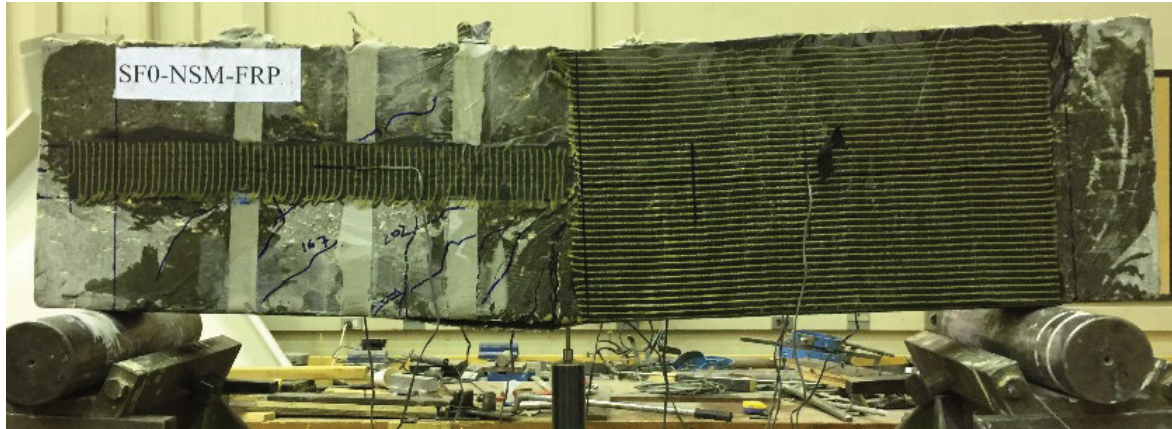


Fig. 5. Failure pattern of specimen DB-FRP

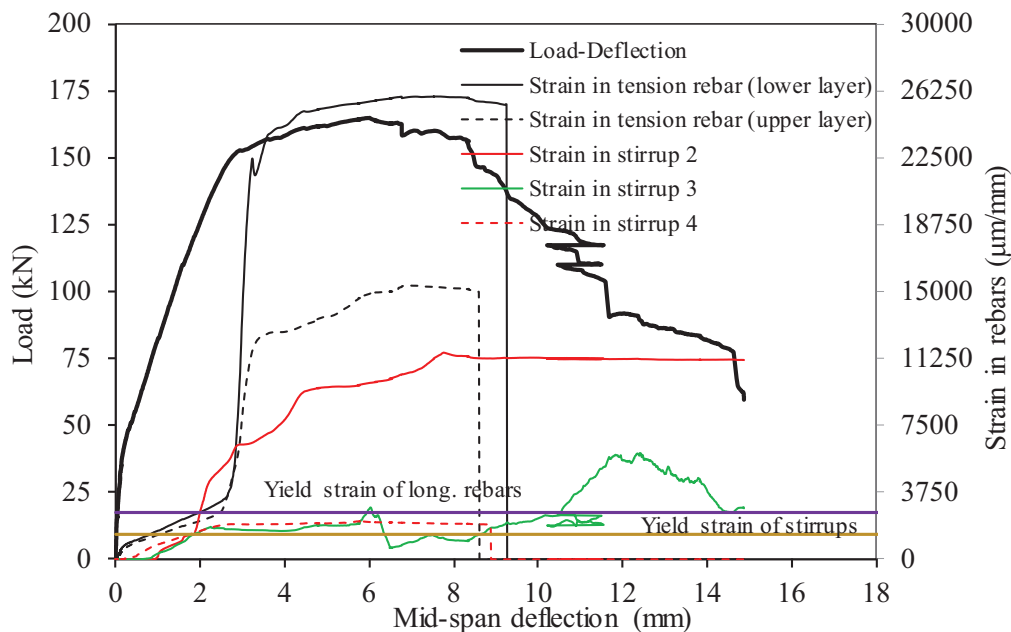


Fig. 6. Load displacement of specimen DB-S-F

flexural failure crack appeared in the middle of the beam span.

3.2. Load-displacement response and strains

Figures 7–9 display load-displacement relationship for various kinds of test specimens. Strains in longitudinal rebars, FRP strips, and/or shear stirrups are also shown in these diagrams to help interpret the observed behavior change. The shear

stirrups and FRP strips referred to here have the same numbers displayed in Figure 2.

3.2.1. DB-S-F specimen

The load steadily grew as the beam's mid-span deflection continued, as seen in Figure 6, until it reached around 151 kN. Both the top and bottom longitudinal rebars were yielding at this stage, and the shear stirrups yielded 0.71 times the ultimate load (P_u), as illustrated in Figure 8. After this step, the beam continued to acquire strength, albeit with

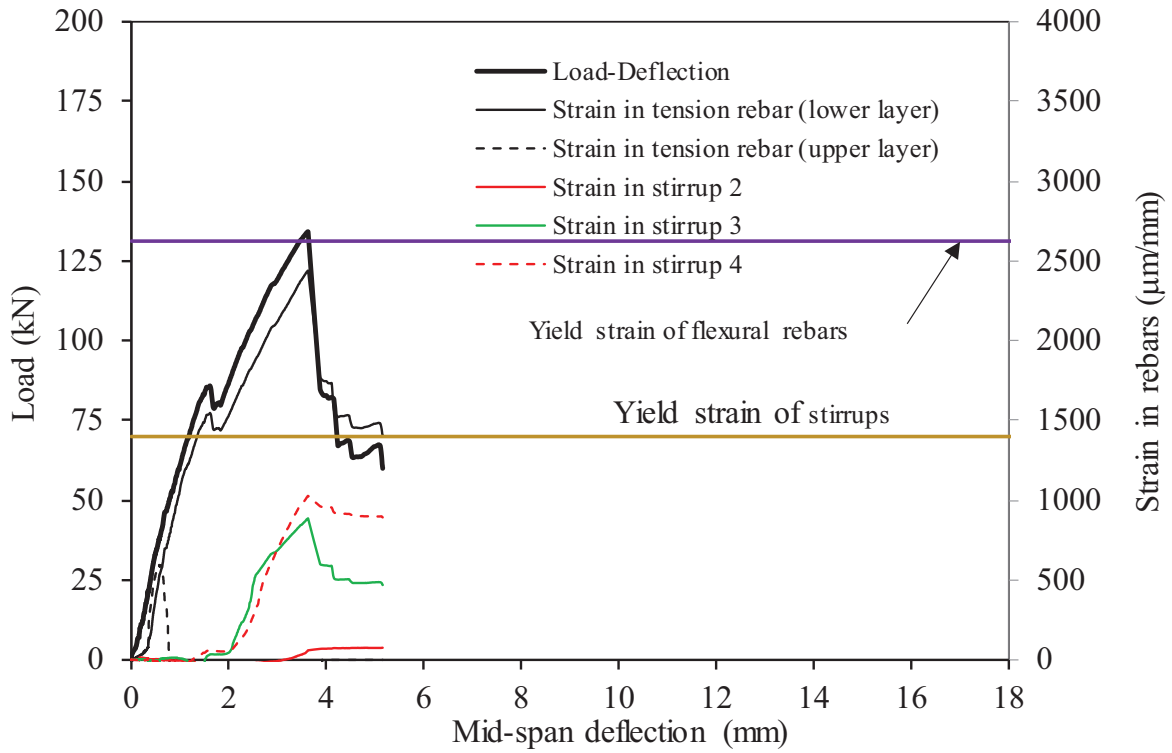


Fig. 7. Load displacement of specimen DB-NS0

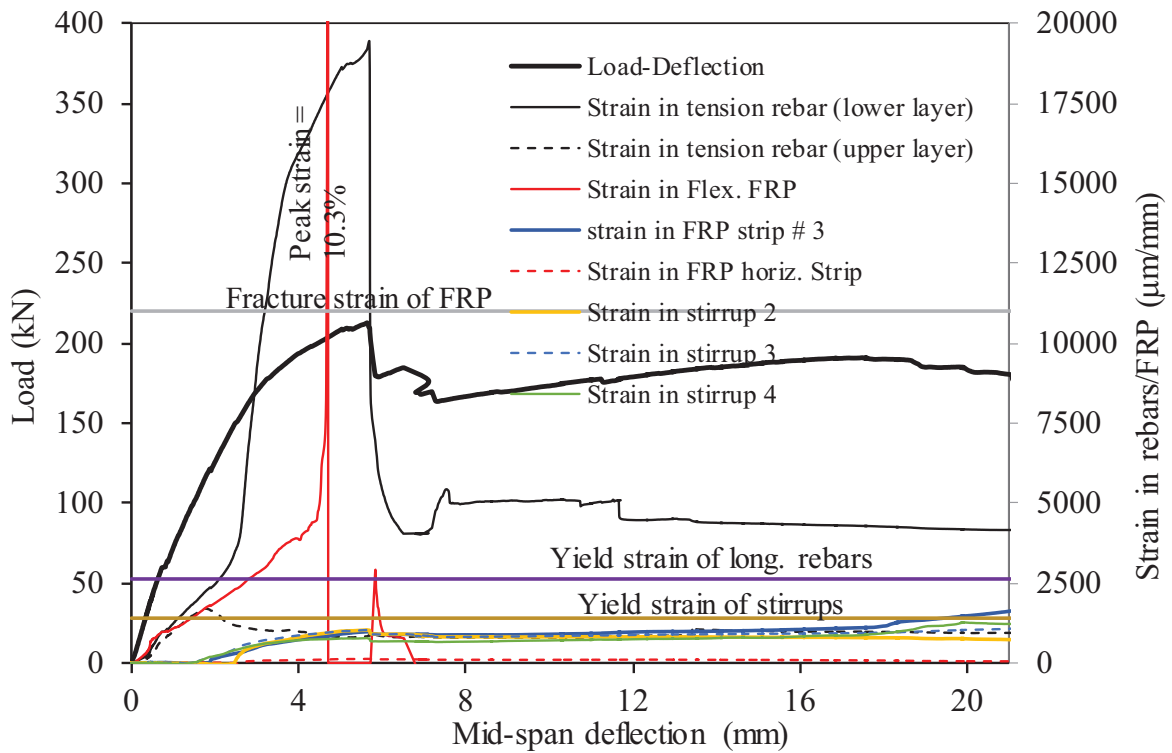


Fig. 8. Load displacement of specimen DB-S

lower stiffness, until it achieved the peak load of 164.2 kN. The strain in the main longitudinal rebar was approximately 1.1% at this point. Following that, the beam exhibited protracted inelastic behavior with a stable strength reduction. While the peak reaction was primarily impacted by a substantial shear crack, the post-peak curve shows indications of significant flexural contribution.

3.2.2. DB-NS0 specimen

The load exhibits an almost linear increase as the mid-span deflection increases until a sharp decrease in load occurs at around 85.6 kN. This drop is attributed to the formation of a significant shear crack on the unreinforced side of the beam, as shown in Figure 7. Subsequently, the load continues to rise until it reaches a maximum load of 134.2 kN. The increase in load is associated with the widening of the shear crack, followed by another drop in load, leading to the failure of the beam due to further crack widening and separation of the shear crack faces.

The maximum strain experienced by longitudinal rebars of the bottom layer is 2440 $\mu\text{m}/\text{mm}$, which is well below the yield threshold. However, the maximum strain in longitudinal rebars of the top rebars is only 595 $\mu\text{m}/\text{mm}$, which is a significant reduction from the overall strain. The other half of the span's shear stirrups also show minimal strain. Since the shear cracks are confined to the unreinforced section of the beam, this result is to be anticipated.

3.2.3. DB-FRP specimen

There are two distinct regions in the deep beam's load versus displacement fluctuation from the base to the peak: elastic up to 48 kN and non-linear up to the maximum load of 224 kN. As can be seen in Figure 8, the load increased smoothly with the beam's mid-span deflection up to a value of roughly 224 kN. Figure 8 shows that the yield strain has been exceeded in both the bottom layer of flexural reinforcement and shear stirrups 3 and 4. After this point, the beam's strength increased but its stiffness decreased, and this trend persisted until the peak load of 224 kN was reached.

After the maximum stress was reached, the material remained in a plastic state with a gradually decreasing strength. The post-peak curve shows that flexural cracks predominated in the reaction after the peak. Compared to the horizontal FRP strip provided at mid-depth, the strain in vertical NSM CFRP U-wrap was lower. The flexural FRP strip had a strain that was significantly higher than the fracture strain. The adopted NSM FRP strips scheme provides considerable enhancement, and it was more effective in increasing deep beam shear resistance and ensuring larger deformation capacity. The results are consistent with previous studies [23, 27].

4. Performance of strengthening scheme

Table 5 provides a summary of the ultimate loads obtained from the tested deep beams. For specimens with stirrups, the steel web reinforcement alone contributes to 23% of the shear resistance compared to deep beams without stirrups. The implementation of the NSM strengthening strategy in the DB-FRP specimen successfully prevented shear failure in the section without stirrups, thereby shifting the failure mode to flexural failure. The inclusion of the NSM scheme in DB-FRP had significant peak shear strength and slight improvement in the displacement capacity of the deep beam. In comparison to the reference specimens, the NSM strengthening system exhibited a

Table 5. Test results of all tested specimens

Beam description of half span part	Shear strength (kN)	Note
Beam part with no stirrups	67.1 (DB-NS0)	–
Beam part having stirrups in all span	82.5 (DB-S-F)	23% improvement as compared to DB-NS0
RC beam part with no stirrups but strengthened using NSM U-wrap CFRP strips	112 (DB-FRP)	82% improvement as compared to DB-NS0

Table 6. Constitutive material models parameters of concrete, Sikadur resin, and CFRP

Material	Parameters	Values	Denotation
Concrete	Dilation angle (ψ)	32°	Calibrated value
	Eccentricity (ϵ)	0.1	ABAQUS (default value)
	Stress ratio (σ_{b0}/σ_{c0})	1.16	ABAQUS (default value)
	Shape factor (K_c)	0.667	ABAQUS (default value)
Sikadur mortar	Dilation angle (ψ)	40°	Calibrated value
	Eccentricity (ϵ)	0.1	ABAQUS (default value)
	Stress ratio (σ_{b0}/σ_{c0})	1.16	ABAQUS (default value)
	Shape factor (K_c)	0.667	ABAQUS (default value)
CFRP sheet	Poisson's ratio (ν)	0.3	Widely used in FE modeling
	Modulus of Elasticity (E)	230000 MPa	Given by the manufacturer
	Tensile strength (longitudinal: σ_{t1})	1122 MPa	Experimental Value
	Compressive strength (longitudinal: σ_{c1})	10 MPa	Al-Mekhlafi, et al. [11]
	Shear strength (longitudinal: τ_{f1})	10 MPa	
	Transversal tensile strength (σ_{t2})	10 MPa	
	Compressive strength (transversal: σ_{c2})	10 MPa	
	Shear strength (transversal: τ_{f2})	10 MPa	

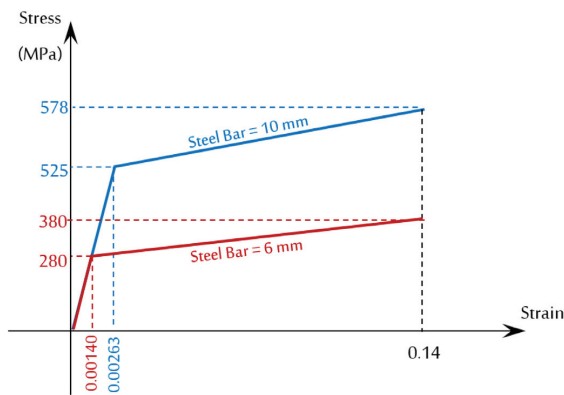


Fig. 9. The idealized stress-strain curve for steel reinforcement

notable enhancement in the ultimate capacity, with a gain percentage ranging from 82%, as indicated in Table 5. This illustrates the effectiveness of the NSM application in enhancing the shear strength of RC deep beams.

5. Finite element modeling

RC deep beams have been modeled using the nonlinear 3D finite element software ABAQUS [30]. The FE model's accuracy was verified by comparing them with the experimental test findings of this study.

5.1. Constitutive material models

The concrete damaged plasticity (CDP) model, widely employed in FE investigations (e.g., [31–33]), was utilized to predict the behavior of concrete and Sikadur resin mortar materials. The CDP model includes isotropic damaged elasticity and compressive and tensile plasticity to effectively represent the plastic responses [1]. Hognestad [34] developed a compressive concrete model for non-linear FE investigations. Moreover, Stoner [35] modified the curve to account for the influence of concrete confinement by introducing stirrups and the ultimate concrete strain. This study used this model to represent the stress-strain behavior of concrete under compression. When modeling tension behavior in concrete, it is noted that before reaching fracture stress, the behavior is linear and elastic, showing a steady stress increase. Following this, a gradual decrease in the stress-strain curve is noted, representing a decrease in concrete strength. The current study employed the model developed by Wang and Hsu [36] for modeling the stress-strain curve of concrete under tension. The failures in tension and compression were represented using the DAMAGET and DAMAGEC options, which were specified during the modeling phase [30]. Table 6 presents the material parameters employed in the concrete and Sikadur mortar materials within

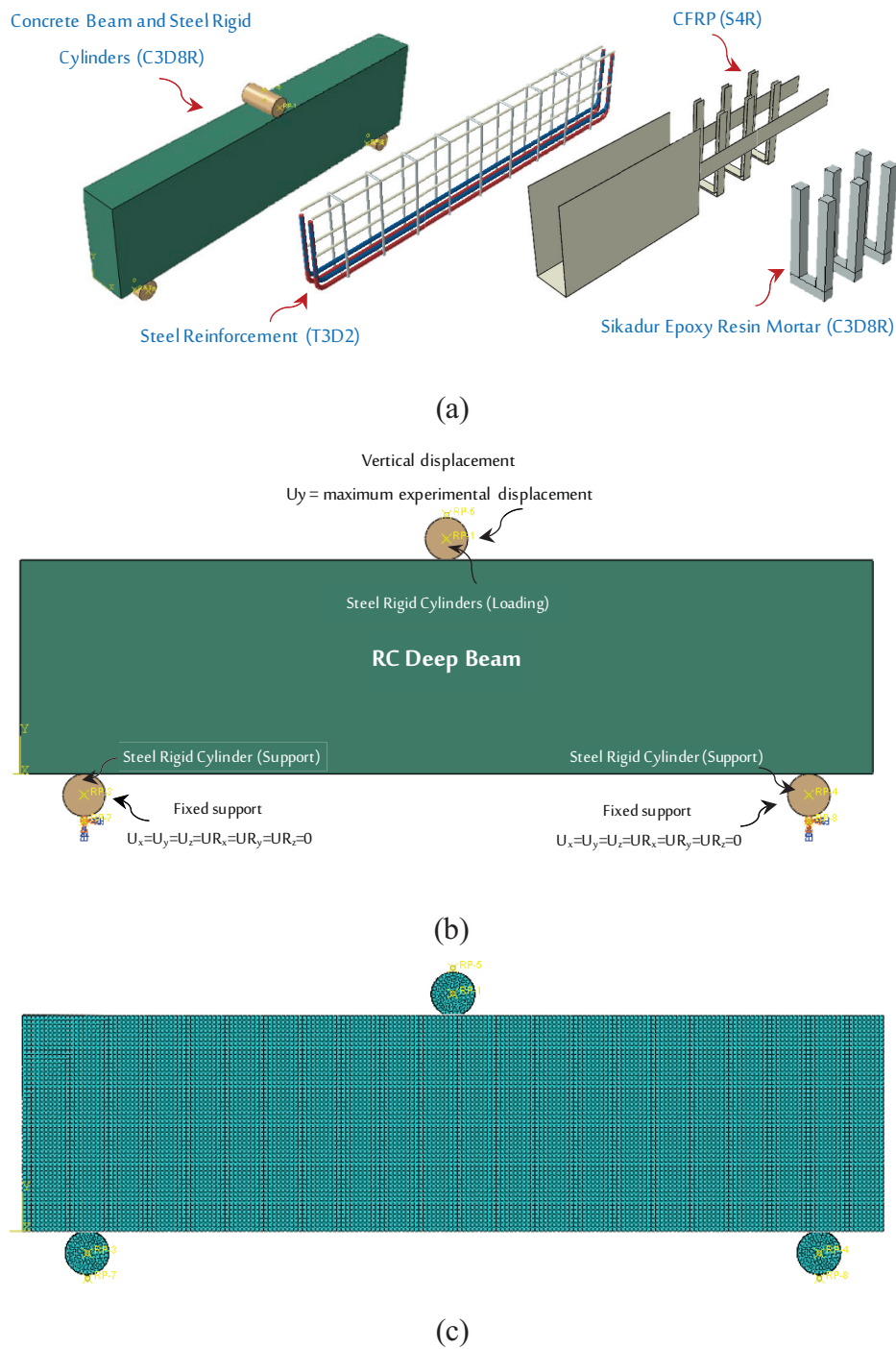


Fig. 10. FE model set-up: (a) Finite elements types; (b) Loading and boundary conditions; (c) Meshing size.

the context of the CDP. Titoum et al. [37] developed idealized stress-strain curves to model the behavior of steel reinforcement in the FE investigations, shown in Figure 9. The FRP material (i.e.,

CFRP) was modeled as having linear behavior, as demonstrated in other research [38, 39]. The composite laminate mode was utilized to simulate the CFRP sheets available in the ABAQUS

Table 7. Mesh convergence analysis results

Mesh types	Beam elements size	Experimental flexural strength (kN)	FE flexural strength (kN)	Experimental/FE
Type 1	25	165	185	89.2%
Type 2	15		178	92.7%
Type 3	7		172	95.6%

Table 8. Comparison of experimental and FE results

Specimen ID	Exp. flexural strength (kN)	FE flexural strength (kN)	Error %
DB-S-F	165	172	4.07%
DB-NS0	134	137	2.19%
DB-FRP	212	218	2.75%

software [30]. Table 5 presents the FRP material parameters employed in the FE investigation.

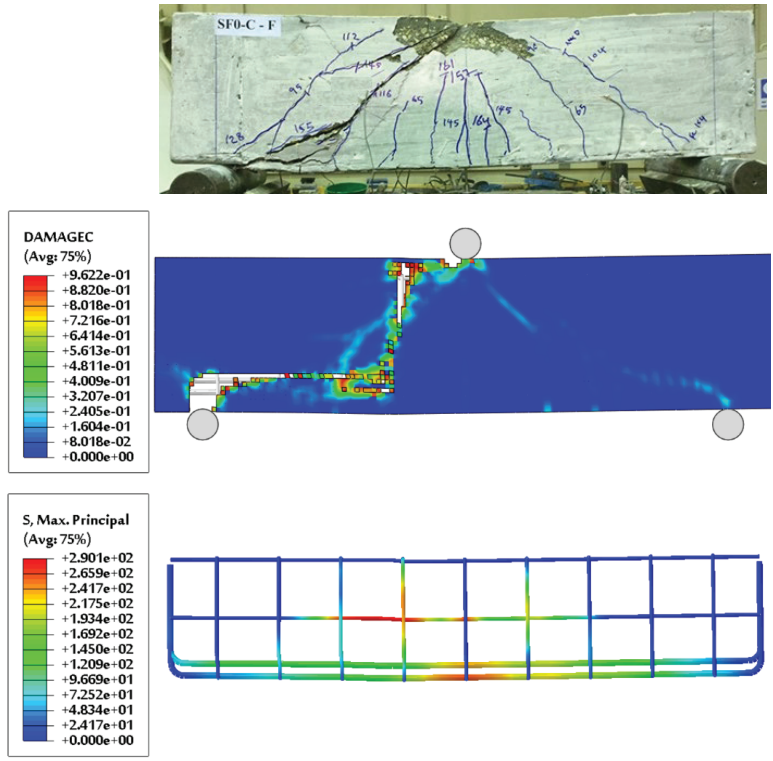
5.2. FE model set-up

Figure 10(a) depicts the utilization of the eight-node element (C3D8R) to simulate the concrete and Sikadur mortar components. The longitudinal reinforcing bars and stirrups were depicted using a two-node and linear truss element, denoted as T3D2, as illustrated in Figure 10(a). The simulation of CFRP sheets was conducted with a shell element known as S4R, which is a three-dimensional structure consisting of four nodes. The modeling of the supports was conducted by applying a boundary condition at the reference points (RP) that attach to the lower supporting cylinders, as depicted in Figure 10(b). Displacement control was employed to gradually apply the load, utilizing the two RPs assigned to the top cylinder, as depicted in Figure 10(b). The perfect bond and interface element approaches were employed by the researchers to simulate the interfaces of the NSM [12–17]. The experimental testing did not reveal significant separation or debonding at the interfaces between the concrete, Sikadur mortar, and NSM components. Hence, the assumption of a successful bond was made in the FE modeling [40–44]. According to the findings of Banjara and Ramanjaneyulu [45], it was demonstrated that the utilization of the perfect bond yielded more accurate FE outcomes

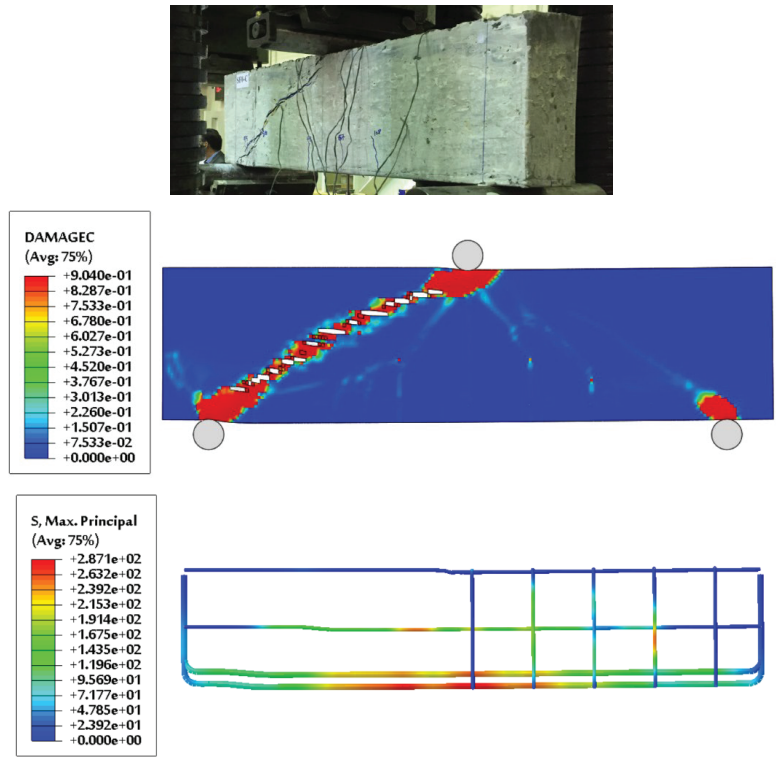
in comparison to the interface element, as evidenced by the experimental result comparison. In this study, the embedded function was employed to simulate the interactions between the concrete and steel reinforcement, as well as between the Sikadur mortar and CFRP components. The strong bond between epoxy and concrete is a consequence of the adhesive qualities of epoxy. The failure of either the concrete elements or the epoxy directly influences the total failure of the system. The mesh convergence analysis was carried out on the DB-S-F specimen using three different meshing types. The geometry, element types, and material properties remain consistent across the modeling process of the three meshing types. The results of the three meshing types are illustrated in Table 7. A comparison of the three meshing types was made to choose the appropriate mesh size. In comparison to the experimental findings, the use of mesh type 3 produced higher convergence and more accurate outcomes, as shown in Table 7. The use of a finer mesh than mesh type 3 necessitated increased allocation of resources and computer running times without achieving any convergence improvement. Finally, a mesh size of 7 mm was chosen due to its ability to produce satisfactory outcomes when compared to the experimental data, as depicted in Figure 10(c).

5.3. Numerical results and verifications

In this section, a numerical validation of the experimental findings is presented. Table 7 provides a summary of the obtained results, whereas Figure 11 illustrates the failure modes, and Figure 12 presents the load-deflection curves. The FE models have exhibited the capacity to predict with accuracy the failure patterns observed in experimental tests of RC deep beams exposed to flexural loads using different strengthening techniques. A



(a)



(b)

Fig. 11. Continued

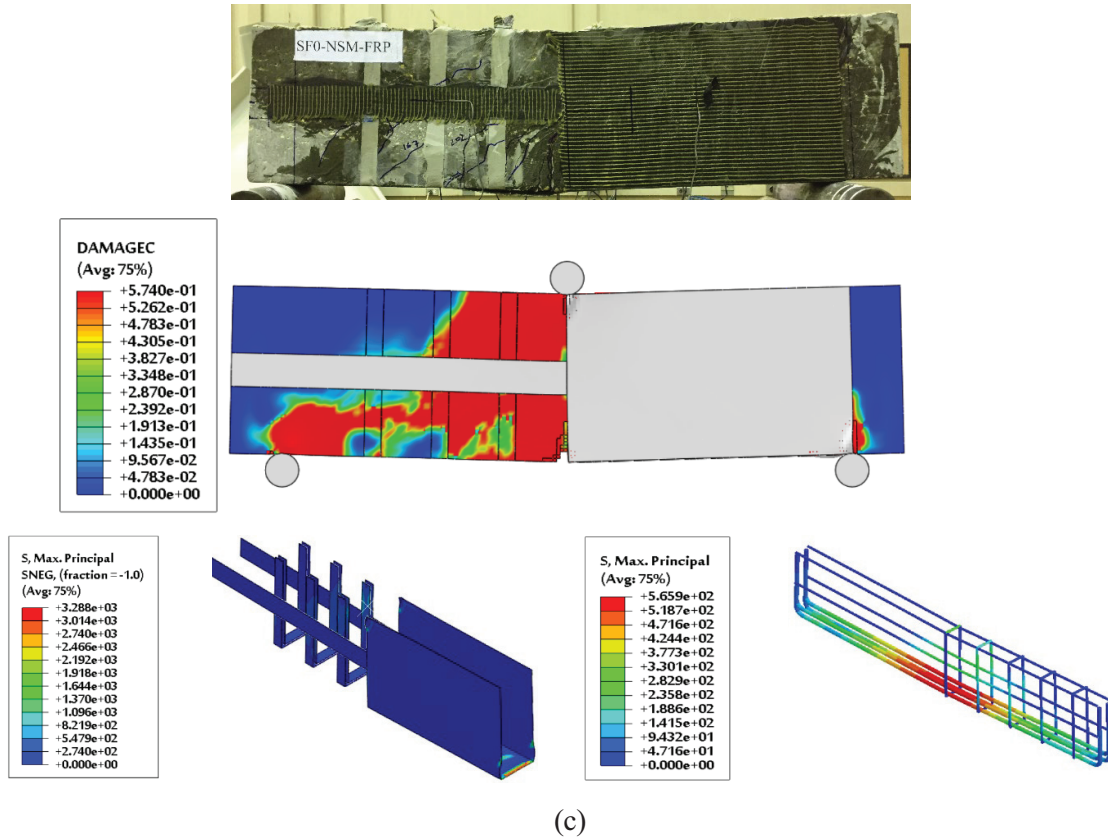


Fig. 11. Failure modes for FE and experimental deep beams: (a) DB-S-F; (b) DB-NS0; (c) DB-FRP

comparison between the failure modes of experimental and FE outcomes for all specimens is illustrated in Figure 11. The observed deformation patterns and stress graphs in the FE models exhibit similarities to the experimental findings. Figure 12 illustrates a comparison of the load-deflection curves obtained from the FE models and the experimental findings. The agreement level between the experimental and FE outcomes is considered acceptable. The FE model accurately represents the maximum loads recorded by the experimental specimens, as shown in Table 8. The variation seen between the FE models and experimental results is within a satisfactory range. According to the results shown in Table 6, it is evident that the highest deviation between the FE and experimental outcomes reached approximately 6%. The simulated FE models exhibited variations from the experimental specimens in certain instances. The observed variances in the FE curves

and failure mechanisms can be attributed to the flawless performance exhibited by the FE specimens throughout the modeling procedures. The FE simulation utilized in this investigation was unable to totally adequately account for the initial concrete weaknesses, such as nonuniformity, deterioration, and early cracking. In summary, the simulation outcomes have presented substantial confirmation for the dependability of the FE models, thereby demonstrating their appropriateness for producing further predictions.

The integration of experimental tests and Finite Element modeling (FEM) yields a thorough comprehension of the load-displacement characteristics of deep beams. The FE model of the DB-S-F specimen showed very satisfactory results compared to the results of the experimental test, where both curves were almost the same up to the highest resistance, then the FE curve showed values slightly higher than the experimental curve.

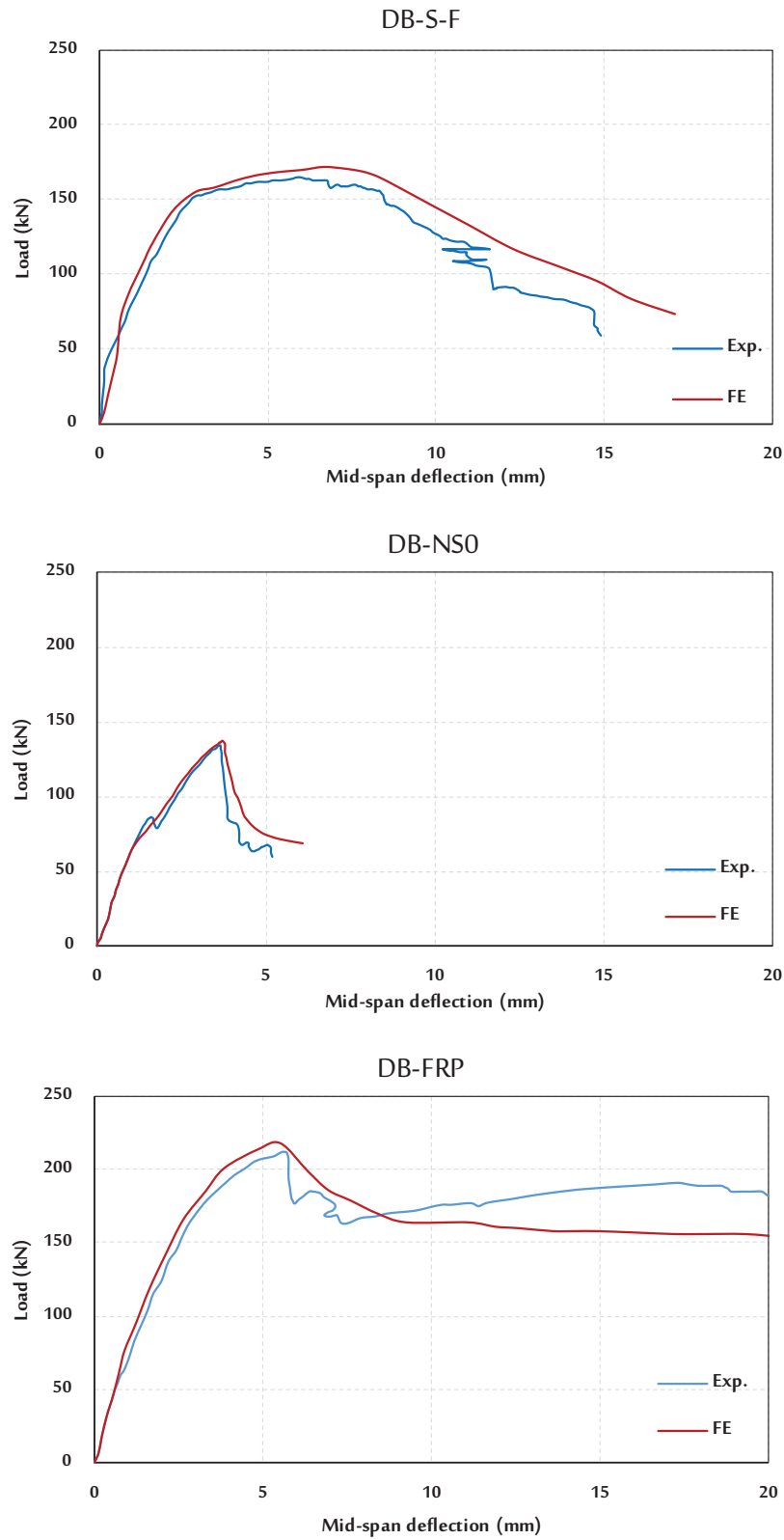


Fig. 12. FE and experimental load versus mid-span deflection curves for deep beams

The same trend was noticed in the FE model of the DB-NS specimen. For the FE model of the DB-FRP specimen, the FE curve showed values lower than the experimental curve. It is worth mentioning that the FE modeling curves did not illustrate any small breaks that were observed in the experimental curves. The observed variances in the FE curves can be attributed to the flawless performance (such as nonuniformity, deterioration, and early cracking) exhibited by the FE specimens throughout the modeling procedures.

6. Conclusions

The study yields the following significant findings:

- Unlike the brittle diagonal shear failure observed in the unstrengthened beam, the inclusion of NSM FRP sheets filled with epoxy resin promoted a ductile flexural-shear failure mode.
- Beams that were reinforced in shear using NSM U-wrap CFRP sheets exhibited an 82% enhancement in shear capacity compared to the control beam.
- Observations indicated that the addition of web reinforcement led to a shear strength improvement ranging around 23% when compared to beams without shear stirrups.
- While the typical failure mode for NSM FRP strengthened RC normal beams involves the interface between the NSM FRP reinforcement and adhesive layer, no instances of damage failure were observed in the NSM strengthening technique for deep beams.
- The utilization of the NSM technology using CFRP laminates has demonstrated its success in enhancing the shear resistance and deformation capacity of RC deep beams.
- The 3D FEM developed in this work showed reasonable agreement with experimental results, accurately simulating the load-displacement behavior and failure modes of

the unstrengthened and strengthened deep beams with the NSM FRP scheme.

- Additional research is required to examine the extended-term effectiveness and durability of RC deep beams reinforced using NSM CFRP laminates, specifically when subjected to continuous loads and environmental conditions.

Acknowledgments

The authors extend their appreciation to Researchers Supporting Project number (RSP2024R343), King Saud University, Riyadh, Saudi Arabia.

References

- [1] Li L, Khan M, Jiang X, Shakor P, Zhang Y. Editorial sustainable fiber reinforced cementitious composites for construction building materials. *Front Mater.* 2023;10:1–2. Available from: <https://doi.org/10.3389/fmats.2023.1237960>.
- [2] Shakor, P. N., & Pimplikar, S. S.. Glass fibre reinforced concrete use in construction. (2011). *Int. J. Technol. Eng. Syst.*, 2(2), 6.
- [3] Abbas H, Almusallam T, Al-Salloum Y, Siddiqui N, Abadel A. TRM versus FRP as strengthening material for improving impact resistance of RC slabs. (2016). Available from: <https://doi.org/10.1115/OMAE2016-54737>.
- [4] Al-Nimry HS, Ghanem AM. FRP confinement of heat-damaged circular RC columns. *Int J Concr Struct Mater.* 2017;11:115–133. Available from: <https://doi.org/10.1007/S40069-016-0181-4/FIGURES/14>.
- [5] Mohamed OA, Kewalramani M, Khatatb R. Fiber reinforced polymer laminates for strengthening of RC slabs against punching shear: a review. *Polymers (Basel)*. 2020;12:685. Available from: <https://doi.org/10.3390/polym12030685>.
- [6] Dias SJE, Barros JAO. Shear strengthening of RC beams with NSM CFRP laminates: Experimental research and analytical formulation. *Compos Struct.* 2013;99:477–490. Available from: <https://doi.org/10.1016/J.COMPSTRUCT.2012.09.026>.
- [7] Shakor P, Nejadi S, Gowripalan N. Effect of heat curing and E6-Glass Fibre reinforcement addition on powder-based 3DP cement mortar. *RILEM Bookseries.* 2020;28:508–515. Available from: https://doi.org/10.1007/978-3-030-49916-7_52/FIGURES/4.
- [8] Tahwia AM, Noshi A, Abdellatif M, Matthana MH. Experimental investigation of rubberized concrete slab-on-grade containing tire-recycled steel fibers. *Innov Infrastruct Solut.* 2024;9:1–16. Available from: <https://doi.org/10.1007/S41062-023-01354-9/FIGURES/15>.
- [9] Abadel A, Alenzi S, Almusallam T, Abbas H, Al-Salloum Y. Shear behavior of self-consolidating

- concrete deep beams reinforced with hybrid of steel and GFRP bars. *Ain Shams Eng J.* 2023. Available from: <https://doi.org/10.1016/j.asej.2023.102136>.
- [10] Abadel AA, Abbas H, Alshaikh IMH, sennah K, Tuladhar R, Altheeb A, Alamri M. Experimental study on the effects of external strengthening and elevated temperature on the shear behavior of ultra-high-performance fiber-reinforced concrete deep beams. *Structures.* 2023;49:943–957. Available from: <https://doi.org/10.1016/J.ISTRUC.2023.02.004>.
- [11] Abadel A, Abbas H, Almusallam T, Alshaikh IMH, Khawaji M, Alghamdi H, Salah AA. Experimental study of shear behavior of CFRP strengthened ultra-high-performance fiber-reinforced concrete deep beams. *Case Stud Constr Mater.* 2022;16:e01103. Available from: <https://doi.org/10.1016/J.CSCM.2022.E01103>.
- [12] Akkaya HC, Aydemir C, Arslan G. Evaluation of shear behavior of short-span reinforced concrete deep beams strengthened with fiber reinforced polymer strips. *Eng Struct.* 2024;299:117145. Available from: <https://doi.org/https://doi.org/10.1016/j.engstruct.2023.117145>.
- [13] Islam MR, Mansur MA, Maalej M. Shear strengthening of RC deep beams using externally bonded FRP systems. *Cem Concr Compos.* 2005 Mar 1;3. Available from: <https://doi.org/10.1016/j.cemconcomp.2004.04.002>.
- [14] Colotti V. Mechanical shear strength model for reinforced concrete beams strengthened with FRP materials. *Constr Build Mater.* 2016 Oct 15;855–865. Available from: <https://doi.org/10.1016/j.conbuildmat.2016.07.146>.
- [15] Elsanadedy HM, Al-Salloum YA, Almusallam TH, Alshenawy AO, Abbas H. Experimental and numerical study on FRP-upgraded RC beams with large rectangular web openings in shear zones. *Constr Build Mater.* 2019;194:322–343. Available from: <https://doi.org/https://doi.org/10.1016/j.conbuildmat.2018.10.238>.
- [16] Li W, Leung CK. Shear span–depth ratio effect on behavior of RC beam shear strengthened with full-wrapping FRP strip. *J Compos Constr.* 2015 Oct 15;20. Available from: [https://doi.org/10.1061/\(ASCE\)CC.1943-5614.0000627](https://doi.org/10.1061/(ASCE)CC.1943-5614.0000627).
- [17] Adhikary BB, Mutsuyoshi H. Behavior of concrete beams strengthened in shear with carbon-fiber sheets. *J Compos Constr.* 2004;8:258–264. Available from: [https://doi.org/10.1061/\(ASCE\)1090-0268\(2004\)8:3\(258\)](https://doi.org/10.1061/(ASCE)1090-0268(2004)8:3(258)).
- [18] Albidah A, Abadel A, Abbas H, Almusallam T, Al-Salloum Y. Experimental and analytical study of strengthening schemes for shear deficient RC deep beams. *Constr Build Mater.* 2019;216:673–686. Available from: <https://doi.org/10.1016/j.conbuildmat.2019.05.024>.
- [19] Zhang Y, Li X, Zhu Y, Shao X. Experimental study on flexural behavior of damaged reinforced concrete (RC) beam strengthened by toughness-improved ultra-high performance concrete (UHPC) layer. *Compos Part B Eng.* 2020;186:107834. Available from: <https://doi.org/https://doi.org/10.1016/j.compositesb.2020.107834>.
- [20] T.T.P.D.' Thesis. Hokkaido University; Sapporo, Japan, Shear resisting mechanism of reinforced concrete beams with CFS as shear reinforcement, 2012.
- [21] Hanoon AN, Jaafar MS, Hejazi F, Aziz FN. Strut-and-tie model for externally bonded CFRP-strengthened reinforced concrete deep beams based on particle swarm optimization algorithm: CFRP debonding and rupture. *Constr Build Mater.* 2017 Aug 30;428–447. Available from: <https://doi.org/10.1016/j.conbuildmat.2017.04.094>.
- [22] Abadel AA, Albidah AS. Investigation of shear reinforcement schemes for RC deep beams. *Arab J Sci Eng.* 2021;46:4747–4763. Available from: <https://doi.org/10.1007/s13369-020-05123-z>.
- [23] Abbas H, Almusallam T, Abadel A, Alenzi S, Al-Salloum Y. Shear strength of functionally graded self-compacting concrete deep beams reinforced with steel and GFRP bars. *Case Stud Constr Mater.* 2023:e01872. Available from: <https://doi.org/10.1016/j.cscm.2023.e01872>.
- [24] Alqarni AS, Albidah AS, Abadel AA. Shear performance of reinforced concrete deep beams using different coarse aggregates under the effect of elevated temperatures. *Case Stud Constr Mater.* 2022;16:e01087. Available from: <https://doi.org/10.1016/j.cscm.2022.e01087>.
- [25] Emara M, Barris C, Baena M, Torres L, Barros J. Bond behavior of NSM CFRP laminates in concrete under sustained loading. *Constr Build Mater.* 2018;177:237–246. Available from: <https://doi.org/10.1016/j.conbuildmat.2018.05.050>.
- [26] Barros JAO, Dias SJE, Baghi H, Ventura-Gouveia A. New shear strengthening configurations of near-surface-mounted CFRP laminates for RC beams. *ACI Struct J.* 2016;113:1275–1287. Available from: <https://doi.org/10.14359/51689029>.
- [27] Jedrzejko MJ, Zhang SS, Ke Y, Fernando D, Nie XF. Shear strengthening of RC beams with NSM FRP. I: Review of strength models. *Adv Struct Eng.* 2022;26:564–586. Available from: <https://doi.org/10.1177/13694332221125832>.
- [28] Chalioris CE, Kosmidou PMK, Papadopoulos NA. Investigation of a new strengthening technique for RC deep beams using carbon FRP ropes as transverse reinforcements. *Fibers.* 2018;6. Available from: <https://doi.org/10.3390/fib6030052>.
- [29] Mukhtar F, Deifalla A. Shear strength of FRP reinforced deep concrete beams without stirrups: Test database and a critical shear crack-based model. *Compos Struct.* 2023;307:116636. Available from: <https://doi.org/https://doi.org/10.1016/j.compstruct.2022.116636>.
- [30] ABAQUS. User Assistance. Dassault Systèmes Simulia Corporation, Providence, Rhode Island, USA., 2019., (2019).
- [31] Alshaikh, I. M., Abadel, A. A., Sennah, K., Nehdi, M. L., Tuladhar, R., & Alamri, M. . Progressive Collapse Resistance of RC Beam–Slab Substructures Made with

- Rubberized Concrete . Buildings, 2022;12:10. Available from: <https://doi.org/10.3390/buildings12101724>.
- [32] Alshaikh IMH, Bakar BHA, Alwesabi EAH, Zeyad AM, Magbool HM. Finite element analysis and experimental validation of progressive collapse of reinforced rubberized concrete frame. Structures. 2021;33:2361–2373. Available from: <https://doi.org/10.1016/J.ISTRUC.2021.06.008>.
- [33] Altheeb A, Alshaikh IMH, Abadel A, Nehdi M, Alghamdi H. Effects of Non-Structural Walls on Mitigating the Risk of Progressive Collapse of RC Structures. *Lat Am J Solids Struct*. 2022;19:1-18. e440. Available from: <https://doi.org/10.1590/1679-78257023>.
- [34] Hognestad E. Study of combined bending and axial load in reinforced concrete members. University of Illinois at Urbana Champaign, College of Engineering, 1951.
- [35] Stoner JG, Polak MA. Finite element modelling of GFRP reinforced concrete beams. *Comput Concr*. 2020;25:369–382. Available from: <https://doi.org/10.12989/CAC.2020.25.4.369>.
- [36] Wang T, Hsu TTC. Nonlinear finite element analysis of concrete structures using new constitutive models. *Comput Struct*. 2001;79:2781–2791. [https://doi.org/10.1016/S0045-7949\(01\)00157-2](https://doi.org/10.1016/S0045-7949(01)00157-2).
- [37] Titoum, M., Tehami, M., Achour, B., & Jaspard, J. P. Analysis of semi-continuous composite beams with partial shear connection using 2-D finite element approach. *Asian J Appl Sci*. 2008;1:185–205. <https://doi.org/10.3923/ajaps.2008.185.205>.
- [38] Seleem MH, Sharaky IA, Sallam HEM. Flexural behavior of steel beams strengthened by carbon fiber reinforced polymer plates – Three dimensional finite element simulation. *Mater Des*. 2010;31:1317–1324. <https://doi.org/10.1016/J.MATDES.2009.09.010>.
- [39] Vilanova I, Torres L, Baena M, Llorens M. Numerical simulation of bond-slip interface and tension stiffening in GFRP RC tensile elements. *Compos Struct*. 2016;153:504–513. <https://doi.org/10.1016/J.COMPSTRUCT.2016.06.048>.
- [40] Alharthi YM, et al. Flexural response and load capacity of reinforced concrete beams strengthened with reinforced mortar layer. *Eng Struct*. 2021;245:11. <https://doi.org/10.1016/j.engstruct.2021.112884>.
- [41] Elsanadedy HM, Almusallam TH, Alsayed SH, Al-Salloum YA. Flexural strengthening of RC beams using textile reinforced mortar – Experimental and numerical study. *Compos Struct*. 2013;97:40–55. <https://doi.org/10.1016/j.compstruct.2012.09.053>.
- [42] Sharaky IA, Baena M, Barris C, Sallam HEM, Torres L. Effect of axial stiffness of NSM FRP reinforcement and concrete cover confinement on flexural behaviour of strengthened RC beams: Experimental and numerical study. *Eng Struct*. 2018;173:987–1001. <https://doi.org/10.1016/J.ENGSTRUCT.2018.07.062>.
- [43] Abdo A, et al. Effect of main and NSM reinforcing materials on the behavior of the shear strengthened RC beams with NSM reinforced HSC layers and bars. *Case Stud Constr Mater*. 2023;18:e02.
- [44] Shakor P, Gowripalan N, Rasouli H. Experimental and numerical analysis of 3D printed cement mortar specimens using inkjet 3DP. *Arch Civ Mech Eng*. 2021;21:1–16. <https://doi.org/10.1007/S43452-021-00209-3/METRICS>.
- [45] Banjara NK, Ramanjaneyulu K. Experimental and numerical study on behaviour of HSFRC overlay strip strengthened flexural deficient RC beams. *Eng Struct*. 2019;198:109561. <https://doi.org/10.1016/J.ENGSTRUCT.2019.109561>.

Received 2024-04-01

Accepted 2024-05-03